



Quantification of carbon monoxide emissions from African cities using TROPOMI

Gijs Leguijt^{1,2}, Joannes D. Maasakkers¹, Hugo A.C. Denier van der Gon², Arjo J. Segers², Tobias Borsdorff¹, and Ilse Aben^{1,3}

¹SRON Netherlands Institute for Space Research, Leiden, The Netherlands

²Department of Climate, Air and Sustainability, Netherlands Organisation for Applied Scientific Research, TNO, Utrecht, The Netherlands

³Department of Earth Sciences, Vrije Universiteit Amsterdam, Amsterdam, the Netherlands

Correspondence: Gijs Leguijt (g.leguijt@sron.nl)

Abstract. Carbon monoxide (CO) is an air pollutant that plays an important role in atmospheric chemistry and is mostly emitted by forest fires and incomplete combustion in for example road transport, residential heating, and industry. As CO is co-emitted with fossil fuel CO₂ combustion emissions, it can be used as a proxy for CO₂. Following the Paris agreement, there is a need for independent verification of reported activity-based bottom-up CO₂ emissions through atmospheric measurements.

5 CO can be observed daily at global scale with the TROPOMI satellite instrument with daily global coverage at a resolution down to 5.5x7 km². To take advantage of this unique TROPOMI dataset, we develop a cross-sectional flux-based emission quantification method that can be applied to quantify emissions from a large number of cities, without relying on computationally expensive inversions. We focus on Africa as a region with quickly growing cities and large uncertainties in current emission estimates. We use a full year of high-resolution WRF-simulations over three cities to evaluate and optimize the performance of
10 our cross-sectional flux emission quantification method and show its reliability down to emission rates of 0.1 Tg CO yr⁻¹. Comparison of the TROPOMI-based emission estimates to the DACCIWA and EDGAR bottom-up inventories shows CO emission rates in northern Africa are underestimated in EDGAR, suggesting overestimated combustion efficiencies. We see the opposite when comparing TROPOMI to the DACCIWA inventory in South Africa and Côte d'Ivoire, where CO emission factors appear to be overestimated. Over Lagos and Kano (Nigeria) we find that potential errors in the spatial disaggregation of national emis-
15 sions cause errors in DACCIWA and EDGAR, respectively. Finally, we show that our computationally-efficient quantification method combined with the daily TROPOMI observations can identify a weekend effect in the road transport-dominated CO emissions from Cairo and Algiers.

1 Introduction

Carbon monoxide (CO) is an air pollutant that is mostly emitted by anthropogenic sources. It is a product of incomplete combustion in for example road transport, residential heating, industry and forest fires (Zhong et al., 2017). CO is a precursor of ozone, and because it reacts with the hydroxyl radical (OH) its presence effectively increases the atmospheric lifetime of methane (Daniel and Solomon, 1998; Jacob, 1999; Wuebbles and Hayhoe, 2002). The concentration of CO is therefore im-



portant for climate modelling. Furthermore, as many processes that emit CO also emit carbon dioxide (CO₂), knowledge of CO emission rates can provide additional information about CO₂ emissions (Wu et al., 2022; Park et al., 2021). The Inter-
25 governmental Panel on Climate Change (IPCC) identified a need for independent verification of the reported greenhouse gas emissions through measurements (IPCC, 2019). From space this is challenging for CO₂ as its long atmospheric residence time results in high background concentrations, making it hard to detect emissions. For this reason, measuring the 'short lived' CO can be a useful alternative (Silva et al., 2013). We present a method to quantify CO emission rates over cities in Africa using TROPOMI satellite observations.

30

As transport (23%) and residential heating (35%) are key contributors to total anthropogenic CO emissions (Zhong et al., 2017), cities are an important source of CO. Urbanisation scenarios predict a growth in both the number of mega-cities and their populations, leading to larger emission rates and increased health risks. Africa is predicted to have a large urbanisation rate in the coming years. Hoornweg and Pope (2017) predict the continent to house five of the ten largest cities by 2100,
35 compared to one of ten today. Africa is also a region for which relatively large uncertainties are present in emission inventories as only a few are dedicated to the region (Keita et al., 2021). Current emission inventories are based on so called bottom-up methods where emissions are estimated by combining activity data (e.g. national fuel consumption statistics) with emission factors and spatially distribute the emission estimates using proxies like population density (Janssens-Maenhout et al., 2019). These bottom-up methods are also used to report country-level greenhouse emission estimates to the United Nations Frame-
40 work Convention on Climate CHange (UNFCCC). However, lack of detailed data results in large uncertainties (Macknick, 2011; Cai et al., 2019; Oda et al., 2019).

Independently of bottom-up methods, emissions can also be estimated by top-down methods where atmospheric concentra-
45 tions are measured and used to infer the corresponding emission rates. Multiple studies have investigated urban CO emissions using ground-based measurements (Badarinath et al., 2007; McKain et al., 2012; Bi et al., 2022). Many studies have also shown the capability of satellite measurements for this specific task (Borsdorff et al., 2020; Tian et al., 2022a; Plant et al., 2022; Wu et al., 2022). For CO, the TROPospheric Monitoring Instrument (TROPOMI) on ESA's Sentinel 5 precursor satellite is of particular interest (Veefkind et al., 2012). It was launched in 2017 and provides daily global coverage with a resolution of 5.5 by 7 km², which makes it suited to investigate city emissions worldwide.

50

An advantage of polar-orbiting satellites is their ability to monitor the entire globe. However, most satellite-based studies of CO so far have focused either on regional inversions (Yumimoto et al., 2014; Qu et al., 2022) or on trends in concentrations (Lama et al., 2019; Park et al., 2021; Hedelius et al., 2021), while only a few studies have tried to quantify emissions from individual cities or point sources (Dekker et al., 2017; Borsdorff et al., 2020). These urban emission quantifications use at-
55 mospheric inversions, which require computationally expensive high-resolution simulations with Chemical Transport Models (CTMs). Although inversions are able to get relatively accurate emission estimates, they are difficult to apply to a large number of sources. To take full advantage of the TROPOMI data, we adjust the mass balance Cross-Sectional Flux (CSF) method,



originally developed for high-resolution point-source quantifications, to be used with TROPOMI data over urban areas. After evaluating the method using atmospheric transport simulations, we use it to estimate emissions from the largest cities in Africa.

60

2 Data & Methods

This section describes the different data products used in development of the Cross-Sectional Flux method and the simulations that were used to calibrate the model. Section 2.6 will show that the method can be successfully applied to simulated data.

2.1 TROPOMI carbon monoxide data product

65 TROPOMI provides total column carbon monoxide concentrations with daily global coverage at 13:30 local time using the shortwave-infrared band (SWIR) at 2305–2385 nm (Veefkind et al., 2012). From the spectral signal, the CO concentration is inferred using the shortwave-infrared CO retrieval (SICOR) algorithm (Borsdorff et al., 2018). We use three years of data (2019–2021) from the operational data product (Landgraf et al., 2018). To assure high quality data, all pixels with a TROPOMI quality flag below 0.7 are removed, leaving data that are cloud-free or only have low altitude clouds. The CO concentration over
70 cloud-free water surfaces is difficult to retrieve, due to the low intensity of reflected light, therefore, we only use observations with a quality flag equal to 0.7 (low altitude clouds) over water. The resulting dataset shows good agreement with ground-based measurements, with a mean difference per station of $2.45 \pm 3.38\%$ to the unscaled Total Carbon Column Observing Network (TCCON, (Wunch et al., 2011)) columns and $6.5 \pm 3.54\%$ to the Infrared Working Group of the Network for the Detection of Atmospheric Composition Change (NDACC-IRWG, (Hannigan, 2011)) measurement stations (Sha et al., 2021).

75 2.2 EDGAR and DACCIWA bottom-up inventories

We use two different bottom-up inventories to compare the TROPOMI emission estimates with: the Emissions Database for Global Atmospheric Research (EDGAR) version 5 (Oreggioni et al., 2021) and the Africa-focused Dynamics-Aerosol-Chemistry-Cloud Interactions in West-Africa (DACCIWA) inventory (Keita et al., 2021). These inventories are also used in our atmospheric transport simulations (Section 2.3). Both inventories provide yearly gridded emission rates at 0.1° resolution
80 up to 2015. Due to its global scope, the EDGAR inventory relies mostly on international statistics and spatial proxies combined with national data while its emission factors are based on IPCC methodology for greenhouse gases (Eggleston et al., 2006) and the EMEP/EEA emission inventory guidebook for air pollutants (Nielsen, 2013). The DACCIWA inventory provides emission rates over the African continent, ranging from -35 to 38° latitude and -25.5 to 63.5° longitude. It uses similar international data but is supplemented by local measurements of emission factors and data from local authorities (Keita et al., 2021). As the
85 DACCIWA inventory characterizes emission from fewer (sub)sectors than EDGAR, we merge different sectors in EDGAR to match those used in the DACCIWA inventory to make them intercomparable. When reporting urban emissions from EDGAR and DACCIWA, we sum emissions over the pixel closest to the city center, its 8 neighbours and all directly attached pixels where the population density exceeds the surroundings by 1.8 standard deviation. Changing the city masks to $0.3 \times 0.3^\circ$ or



0.7x0.7° boxes changes the resulting values by 10-20% for 17 out of 29 cities in EDGAR and 16 out of 29 cities in DAC-
90 CIWA. Although larger deviations up to 50% in densely populated areas like South Africa are observed, the observed patterns
discussed in Section 3 are valid for these masks as well.

2.3 WRF chemical transport model

To test and calibrate our emission quantification approach we apply it to simulated data. We use the Weather Research and
Forecasting (WRF) chemical transport model version 4.1 (Powers et al., 2017), to simulate emissions over Cairo (Egypt),
95 Bamako (Mali) and Lagos (Nigeria) for 2019, using December 2018 as spin-up month. These three African cities form a
diverse set, with Cairo next to the Nile river, Bamako at the boundary of the Sahara desert and Lagos at the coast of the Atlantic
Ocean. We simulate CO as an inert tracer and drive the simulations with meteorological fields from the National Centre for
Environmental Prediction (NCEP, 2000). All simulations have three-layer nested domains where the outer domain covers
2673x2673 km² at a resolution of 27 km; the middle and inner domain cover 891x891 km² at 9 km resolution and 315x315
100 km² at 3 km resolution respectively (Fig. 1). Initial and 6-hourly boundary conditions to capture the background are taken
from the Copernicus Atmosphere Monitoring Service (CAMS) at 0.25°x0.25° resolution, (Inness et al., 2015). The resulting
background is scaled to match the mean background observed by TROPOMI over the full year. We use emissions from the
global Emissions Database for Global Atmospheric Research (EDGAR) version 5 and the Africa-focused Dynamics-Aerosol-
Chemistry-Cloud Interactions in West-Africa (DACCIWA) inventory. City-specific hourly, daily and monthly temporal profiles
105 for each emission sector are taken from Guevara et al. (2021). To maintain flexibility over model output the different sectors in
the emission inventories (19 for EDGAR and 6 for DACCIWA) are simulated separately.

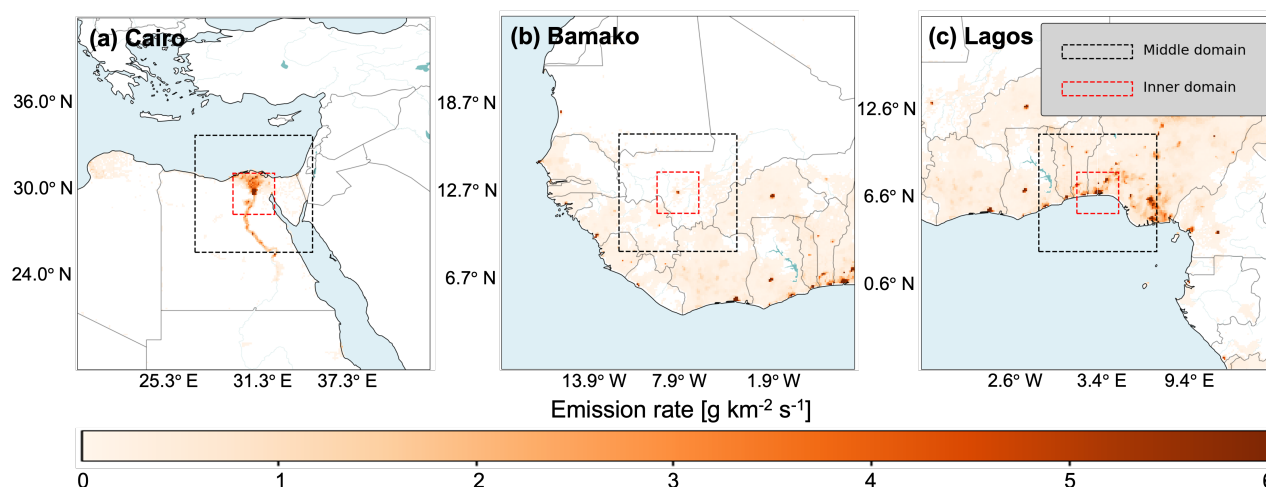


Figure 1. Domain setup of the WRF simulations over Cairo (Egypt), Bamako (Mali) and Lagos (Nigeria). The inner domain (red) spans 315x315 km² around the city at 3 km resolution. The middle (black) and outer (full figure) domain cover 893x893 km² and 2673x2673 km² at 9 and 27 km resolution respectively. All panels also show the emission rates from the DACCIWA inventory.



2.4 Cross-Sectional Flux method

The Cross-Sectional Flux method (CSF) has been shown to be an effective way to quantify emission rates of plumes observed by satellites (Varon et al., 2018, 2020; Sadavarte et al., 2021b; Tian et al., 2022b). It is based on the continuity equation which
110 relates the flux through a closed surface to the associated emission rate:

$$Q = \oint U_{\perp} \Delta\Omega dA, \quad (1)$$

where Q [kg s^{-1}] is the emission rate, U_{\perp} [m s^{-1}] is the wind speed perpendicular to the closed surface, $\Delta\Omega$ [kg m^{-3}] is the enhancement at the closed surface and dA [m^2] is a surface element. As illustrated in Fig. 2A, the plumes have a distinct direction as they move with the wind, they are very directional and it suffices to integrate over perpendicular transects that
115 cover the entire plume-width (Fig. 2B). Equation 1 can then be rewritten as:

$$Q = \int U_{\perp}(x,y) \Delta\Omega(x,y) dy, \quad (2)$$

with x, y coordinates along and perpendicular to the plume respectively as in Varon et al. (2018). Assuming a constant emission rate, transects at different distances downwind of the source should yield the same emission quantification and can be averaged to make the method more robust.

120

We optimize the implementation of the CSF on TROPOMI data for city-like sources. Figure 2A shows a CO-plume observed by TROPOMI over Cairo on April 7th 2019. As expected, the plume follows the 10-m wind direction given by NASA/GMAO GEOS-FP reanalysis data (Molod et al., 2012). We start by determining the quantification point, with respect to which a background box and plume transects are drawn. To make sure the entire plume is downwind, we take the quantification point 0.1°
125 upwind of the city center. The city center is determined by taking the average position of the pixels in DACCIWA with an assigned weight equal to their emission rate. As the wind direction is an important source of uncertainty, the downwind direction from the quantification point can not be solely based on the GEOS-FP reanalysis wind data. Instead, following Sadavarte et al. (2021a), we infer the wind direction from the satellite observations by rotating a box (0.1° width, 0.4° length) from -90 to $+90^{\circ}$ with respect to the reanalysis wind direction. The direction in which this box encloses the highest mean CO
130 concentration is taken as the downwind direction. In the absence of a plume, this method would create a positive bias as it would select the highest enhancement in the noise. Therefore, we use the reanalysis wind direction if the mean enhancement does not exceed 5 ppb. To calculate CO enhancements, we subtract a background calculated as a mean concentration over a $0.4^{\circ} \times 0.4^{\circ}$ square starting 0.2° upwind from the quantification point (Fig. 2B). If this box contains fewer than five valid pixels, we extend it symmetrically with two arcs of a circle of 10° , 20° , 45° up to 60° until there are at least five TROPOMI pixels
135 in the background region (Fig. 2C). We use extension in an arc-like fashion rather than increasing the size of the square to be able to get estimate background values for coastal cities. Retrievals over water are only possible if there are clouds present, hence increasing the size of the background square upwind could result in background pixels far away from the city that are not representative for the local background.



140 After determining the initial direction of the plume, the shape of the plume is determined in two steps. First, we select all
pixels in a downwind box (0.3° width, 0.8° length) that exceed the mean concentration in the surrounding $3^\circ \times 3^\circ$ area by more
than 1.8 standard deviations. We then fit a 2D-spline (0.8° length), starting at the quantification point through the resulting
plume mask. The transects (0.4° width) are drawn perpendicular to the spline, separated by 0.04° . All pixels overlapping with
145 of signal or missing pixels, the plume mask contains fewer than 3 pixels, a spline fit is unlikely to capture the true plume
shape. In these cases, a rectangular box (0.4° width, 0.8° length) is used to draw the transects, as shown in Fig. 2C. We stop
drawing transects if two consecutive lines are more than one standard deviation below the mean estimate of the earlier transects,
indicating the end of the plume. Lines with less than 70% pixel coverage are removed from the estimate as they will not have
a complete integral, resulting in underestimated emissions.

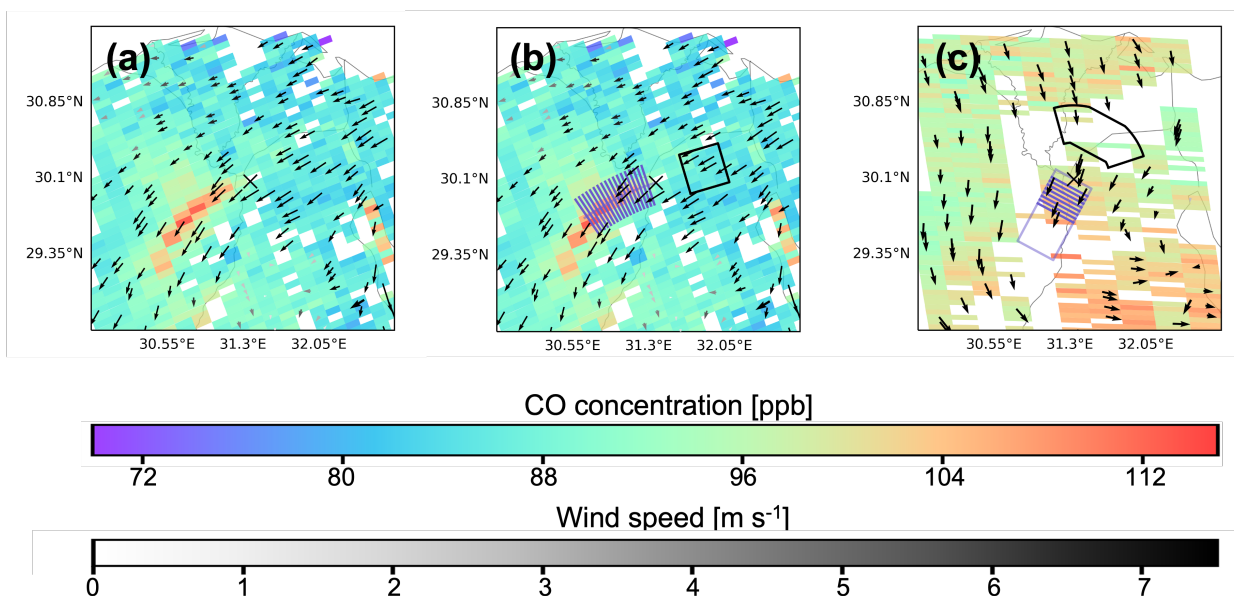


Figure 2. Example of how the cross-sectional flux transects perpendicular to the plume are drawn. (a) TROPOMI data over Cairo on April 7th 2019. The quantification point is shown with a cross and taken 0.1° upwind of the city center. The arrows show GEOS-FP 10-m winds (Molod et al., 2012). (b) Pixels downwind of the city that surpass the regional background by more than 1.8σ form a plume mask through which a 2D spline is fitted (grey line). The transects used for quantification (purple lines) are drawn perpendicular to the spline fit. The background is estimated over the black $0.4^\circ \times 0.4^\circ$ box upwind. (c) TROPOMI observation over Cairo on March 27th 2020. Due to a lack of coverage there are insufficient pixels to generate a reliable plume mask. A rectangular box (grey) is therefore used to draw transects instead. The basic background is extended symmetrically with circle arcs to compensate for a lack of coverage upwind.

150 Using Eq. 2, an emission estimate can be derived for every transect line. Contrary to studies using high-resolution satellites (Varon et al., 2018, 2020), the plumes observed with TROPOMI cover distances over which there can be significant fluctuations in wind speed and direction. We therefore use the wind speed at each transect instead of a single wind speed for the entire plume.



Similar to trends observed in (Sadavarte et al., 2021b), the two lines closest to the quantification point are found to have roughly 30% lower emissions than the lines further away. This pattern is consistent across the cities investigated. One reason is that the
155 early plume only captures part of the city emissions, another explanation is that the associated pixels might see a partial-pixel absorption saturation effect (Pandey et al., 2019). We therefore remove the first two lines from the emission estimate.

2.5 Uncertainty analysis

To estimate the uncertainty of the estimated emission rates, we compile an ensemble of emission estimates for each city. We generate the ensemble by varying parameters of the quantification method such as the wind database used. For example, we
160 vary parameters such as the number of transects and the distance of the background box. To incorporate the uncertainty on the wind data, we use our method with GEOS-FP 10 meter latitude winds, GEOS-FP planetary boundary layer averaged winds (Molod et al., 2012) as well as 10 meter altitude winds from the ERA5 product, provided by the European Centre for Medium-Range Weather Forecasts (ECMWF; (Hersbach et al., 2020)). A complete list of the varied parameters and their ranges can be found in appendix A. For each city, the spread in the resulting ensemble is reported as uncertainty.

165 2.6 Calibration

As simulated (and TROPOMI observed) plumes stay within the inner domain, only the inner domain is used to test the performance of the CSF. A set of synthetic TROPOMI observations is created by sampling the simulation output over the TROPOMI footprints, applying its averaging kernel, selecting pixels based on quality value as discussed in Section 2.1, and adding Gaussian noise with a standard deviation equal to the reported uncertainty of the respective TROPOMI pixel. We also calculate
170 "idealized" pressure weighted columns over the TROPOMI footprints without applying TROPOMI filtering as a first check to see whether the CSF can reproduce the emissions used as model input.

We first test the validity of the CSF method using the idealized columns with 10-m winds output by the WRF simulation. Parameters like the width of the transects are tuned to get optimal quantification estimates on the simulated data. A list of the
175 different parameters and their values can be found in Appendix A. We then use the simulations to calibrate the CSF method following the procedure by Varon et al. (2018). The wind speed in Eq. 2 is replaced by an effective wind speed to account for the effects of turbulence and variation in vertical wind speed and injection height. As the emission rates in the WRF simulations are known, the effective wind can be calculated for every orbit for each of the simulated cities. Figure 3 shows the relation between the effective wind (U_{eff}) and the WRF 10-m winds U_{10} averaged over the plume; the fitted linear relation is:

$$180 \quad U_{eff} = a_{10}U_{10} + b_{10}, \quad (3)$$

with $a_{10} = 1.43$ and $b_{10} = -0.92 \text{ m s}^{-1}$ ($R^2 = 0.82$). U_{10} is the wind speed at the time of overpass at 10 meter altitude. We determine the effective wind relationship separately for the planetary boundary layer averaged winds, which tend to be higher than the surface winds. The resulting calibration gives $a_{PBL} = 0.98$ and $b_{PBL} = -0.20$ ($R^2 = 0.62$). While the absolute value of the PBL winds is closer to the effective wind speeds, using the U_{10} winds captures more of the variability.

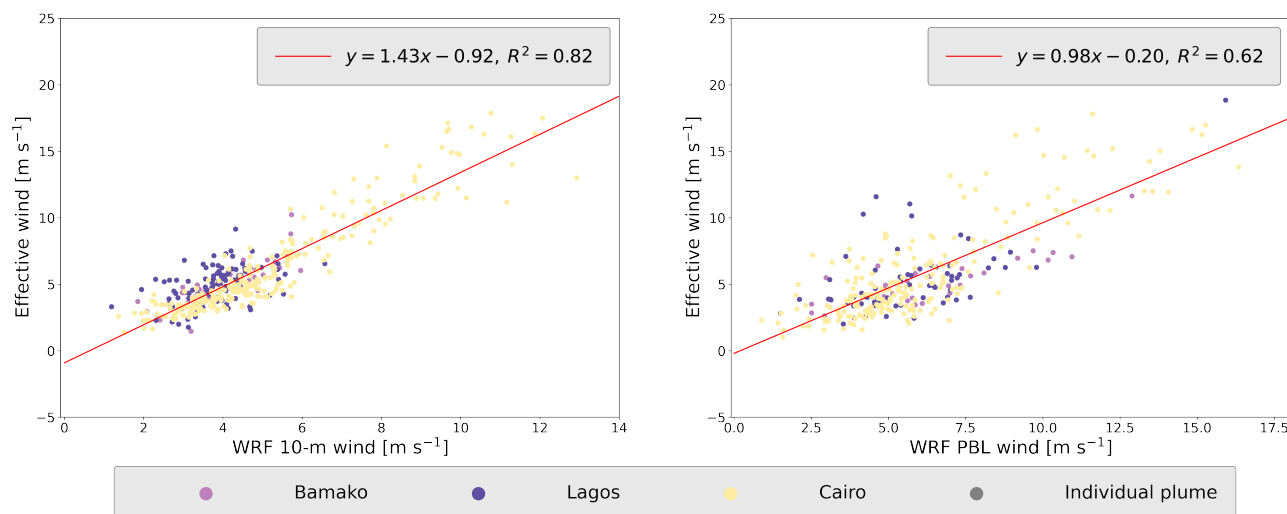


Figure 3. Determination of the relation between the effective wind and both the wind speed at 10 meter altitude (left) and the planetary boundary layer averaged winds (right). The effective wind corrects for the effects of turbulence, injection height and variation in the vertical wind profile. The simulated plumes used in the calibration cover a full year over Cairo, Bamako and Lagos.

185 After determination of the effective wind on plumes with idealized pressure profiles, we test the performance of the CSF on more realistically sampled plumes which include the TROPOMI filtering and averaging kernel. At the same time we test the lower limit to which we can trust the resulting emission estimates, as smaller enhancements are more difficult to distinguish from the background. As the modeled output concentration from the WRF simulations without chemistry scales linearly with the magnitude of the input emissions, simulated city emissions can be scaled up and down without having to rerun the chemical
190 transport model. To do so we use the emission sector most concentrated in the considered urban area to limit the impact of the scaling on the simulated background. Figure 4 shows a comparison between the simulated input and the retrieved emission rates for the three simulated cities. The results suggest that the CSF is able to reproduce input of the WRF simulations when using one year of data for cities with emission rates larger than 0.1 Tg yr⁻¹.

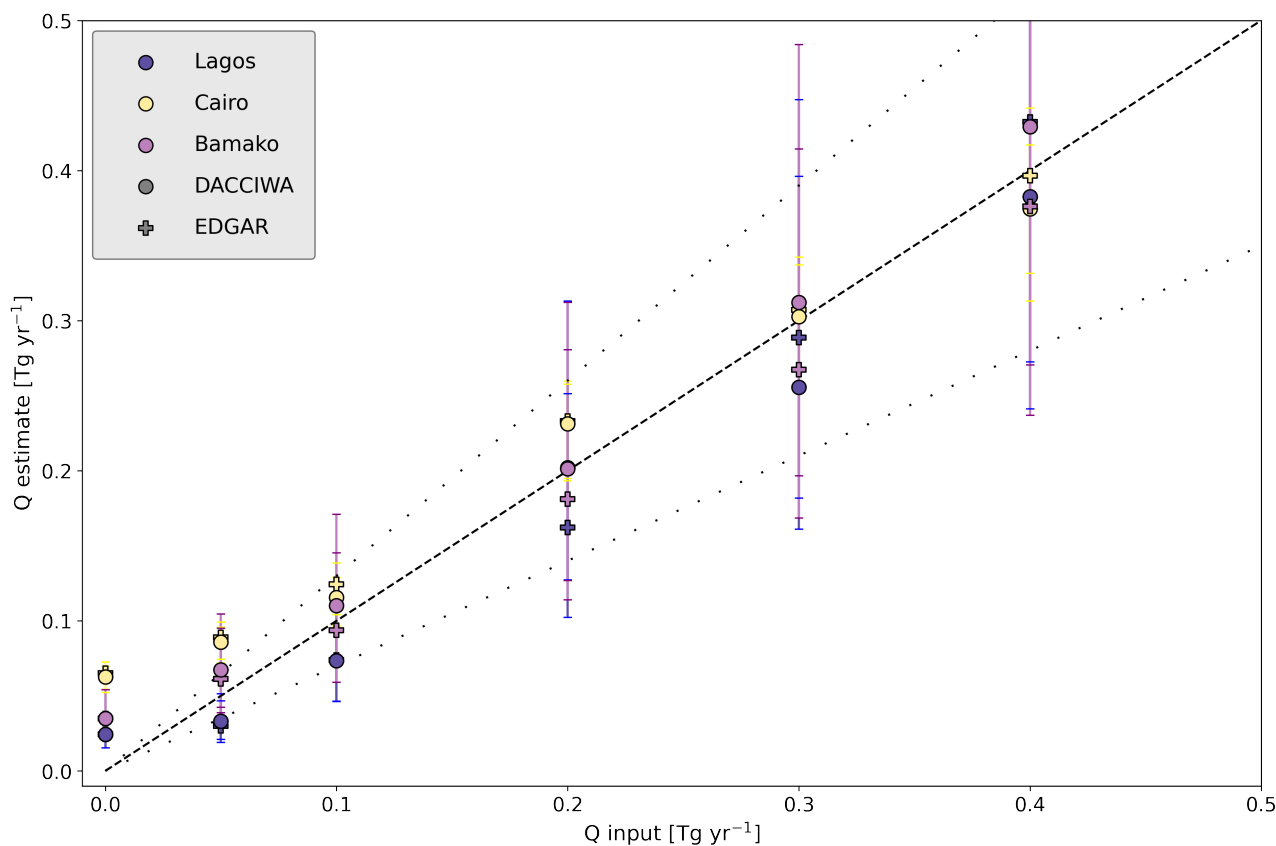


Figure 4. Emission quantification by the CSF on simulated plumes. The plumes are simulated with the WRF-model for the year 2019 over Lagos (Nigeria), Cairo (Egypt) and Bamako (Mali). The simulations either used the EDGAR global bottom-up inventory or the DACCWA inventory. The dotted lines show a 30% deviation from the (dashed) 1:1 line.

To quantify TROPOMI plumes over all major cities in Africa we will use the NASA/GMAO GEOS-FP wind fields (Molod
195 et al., 2012) rather than the WRF simulated wind fields used for the 3 cities selected for evaluation and calibration. Figure
5 shows emission estimates of simulated data using the GEOS-FP wind fields instead of the WRF fields. Individual days are
shown as colored dots, while the mean over the full year is shown as a colored line to represent the average estimate. The
uncertainty of the average is determined as discussed in section 2.5 and shown as a shaded area. The simulation input is shown
as a black dotted line, and lies within the uncertainty of the estimate for both Cairo and Bamako. For Lagos the emission rate
200 is underestimated when using the WRF simulations as the NCEP wind fields that drive the simulations are much higher than
the GEOS-FP and ERA5 wind products specifically over Lagos.

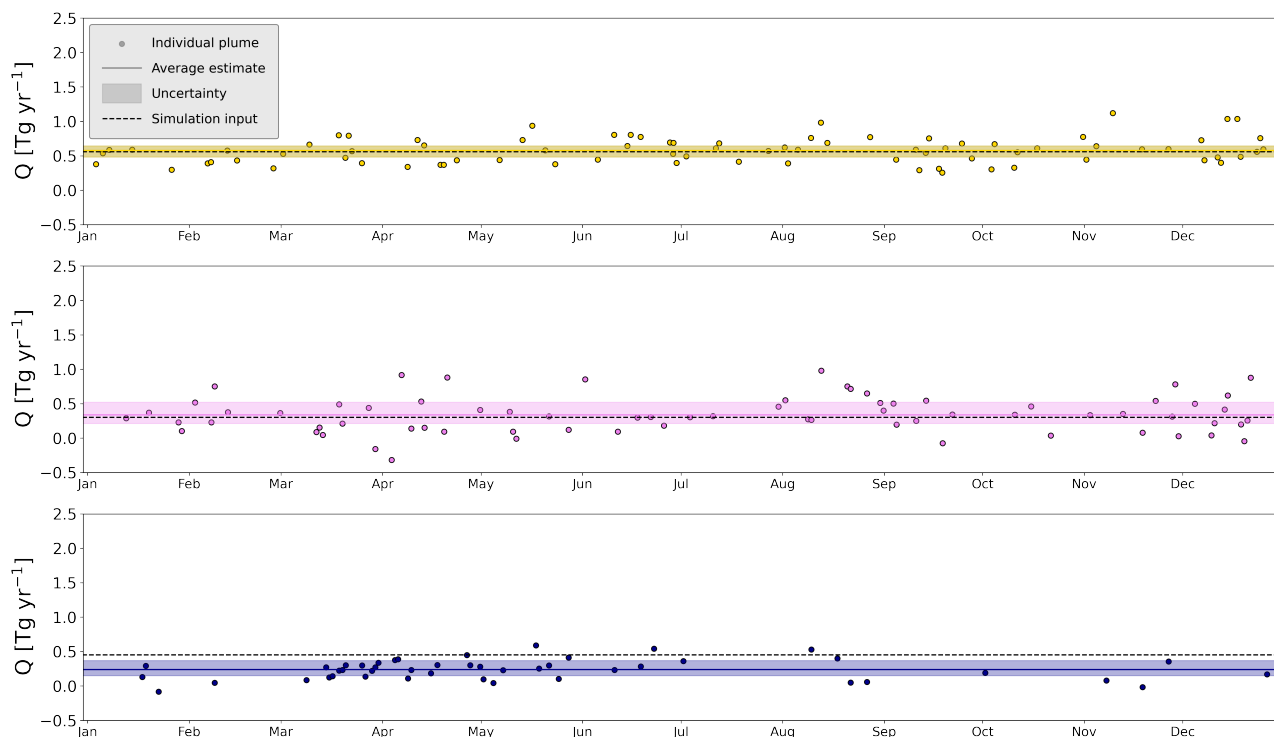


Figure 5. To check the validity of the CSF method for quantification of city emissions we apply the method to simulated plumes sampled as TROPOMI would see them. The dots show CSF emission estimates for individual days over Cairo, Bamako and Lagos respectively. The dark colored line shows the annual CSF mean with the uncertainty based on the emission ensemble shown by the shaded area. The simulation emission input, black dotted line, lies within the uncertainty of the mean CSF emission estimate for Cairo and Bamako showing that the CSF can successfully quantify these urban emissions. For Lagos the emissions are underestimated as the NCEP winds used to drive the simulation are much higher than both the GEOS-FP and ERA5 wind products.

3 Results & Discussion

After verification of the validity and calibration of the method, we apply it to 29 of the largest cities in Africa. These cities are chosen based on their population or because they are emitting above the CSF's quantification threshold in the DACCIWA inventory. Figure 6 shows the results of our TROPOMI quantification and a comparison with the DACCIWA and EDGAR inventories. This data is also included in the appendix in Table D1.

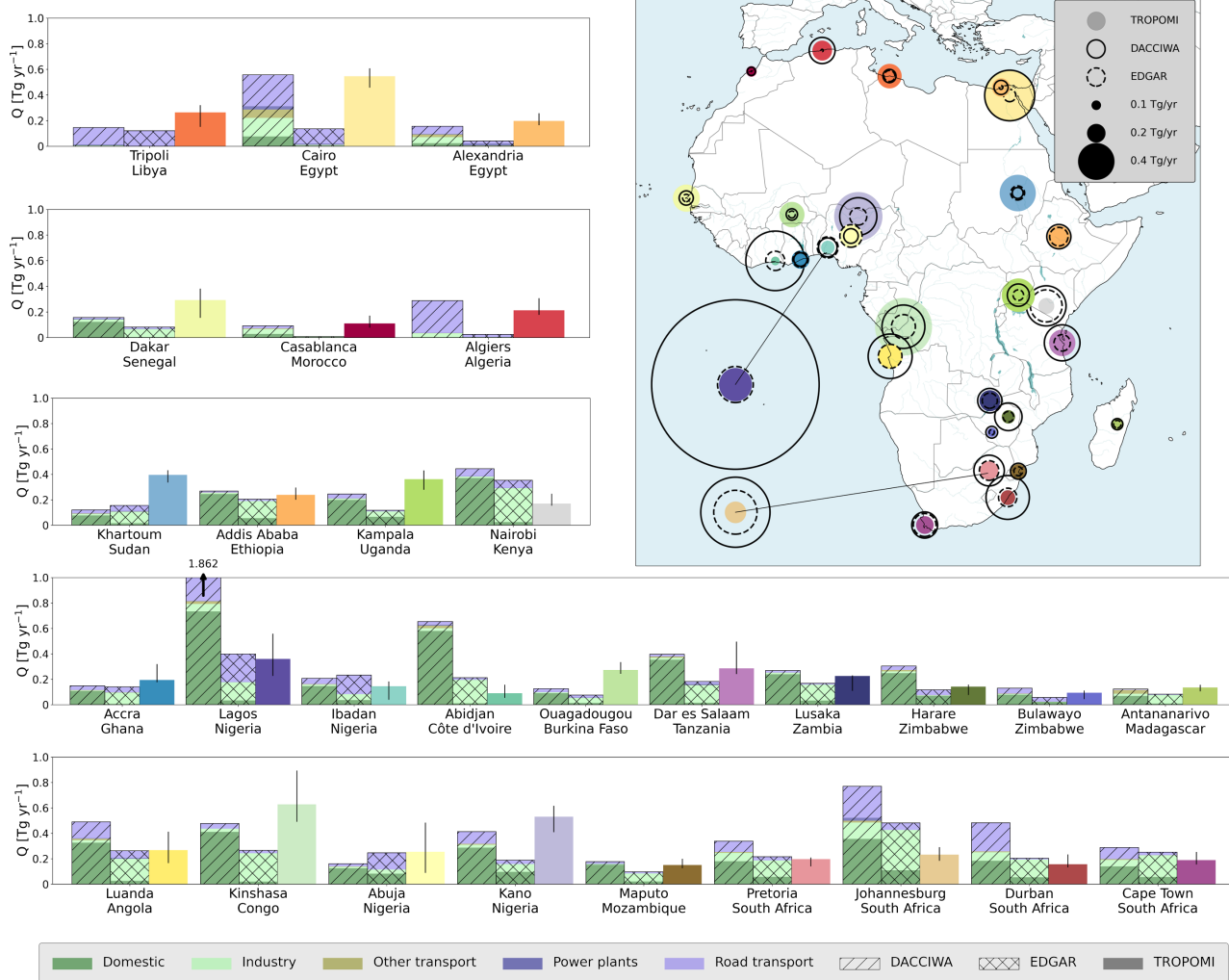


Figure 6. CSF emission quantifications for the largest African cities. Comparison between TROPOMI emission estimates averaged for 2019–2021 (shown as colored circles) and the DACCIWA and EDGAR v5 emission inventories for 2015 shown by the black (dashed) rings. The emission strength is indicated by the size of the circles or rings. The same comparison is made in bar plots where the first two bars show the emission rates from DACCIWA and EDGAR respectively, including the sectoral breakdown. The third bar gives the corresponding TROPOMI estimate where the uncertainty is given by the range of the ensemble. The cities are ordered by geographical location. The emission estimate for Lagos in DACCIWA extends beyond the figure boundary.

On average we find TROPOMI emissions of 0.25 Tg yr^{-1} per city, compared to 0.35 Tg yr^{-1} in DACCIWA and 0.18 Tg yr^{-1} in EDGAR. Except for Abuja (Nigeria) and Khartoum (Sudan), the DACCIWA emission estimates are consistently higher than the EDGAR estimates. Additionally, the two inventories disagree on the sectoral breakdown of the emission estimates with the domestic sector contributing 59% to the total emission rate in DACCIWA while EDGAR attributes 54% of total emissions to the industry sector. For 10 cities TROPOMI and DACCIWA agree within the TROPOMI uncertainty, that is the case for 9 cities



in EDGAR. For 16 cities, the TROPOMI estimates are closer to DACCIWA than to EDGAR. The largest differences between TROPOMI and DACCIWA are found for Abidjan (627%) and Lagos (417%) while estimates for Cairo (2%) and Antananarivo (9%) agree best. To explain the differences between TROPOMI and the inventories we will now focus on some specific areas.

215

Northern Africa

Two cities that stand out in Fig. 6 are Algiers and Casablanca. Unlike DACCIWA, EDGAR does not include any concentrated emissions around these cities, even though they both have populations of 4.2 million. EDGAR also appears to largely underestimate the emissions of the two Egyptian cities that were investigated, Cairo and Alexandria, while the DACCIWA emissions for these cities agree well with our TROPOMI estimates. As we can not directly obtain the underlying emission factors and activity data that are used in EDGAR and DACCIWA, we compare the TROPOMI CO emission rates to the corresponding CO₂ emission rates in EDGAR as shown in Fig. 7. The CO₂ emission rates are also included in Table D2 in the appendix. Cairo, Alexandria, Casablanca and Algiers clearly deviate from the other cities. Their much higher values for CO_{TROPOMI}/CO_{EDGAR} correspond to lower values for CO/CO₂ in EDGAR, indicating that not the activity data but the CO emission factors for these cities are underestimated in EDGAR. This is further confirmed by the fact that the absolute CO₂ emission rates for these cities agree well between the two inventories. The underestimate in CO may point at an overestimated combustion efficiency used in the compilation of the EDGAR emissions for this region.

220

225

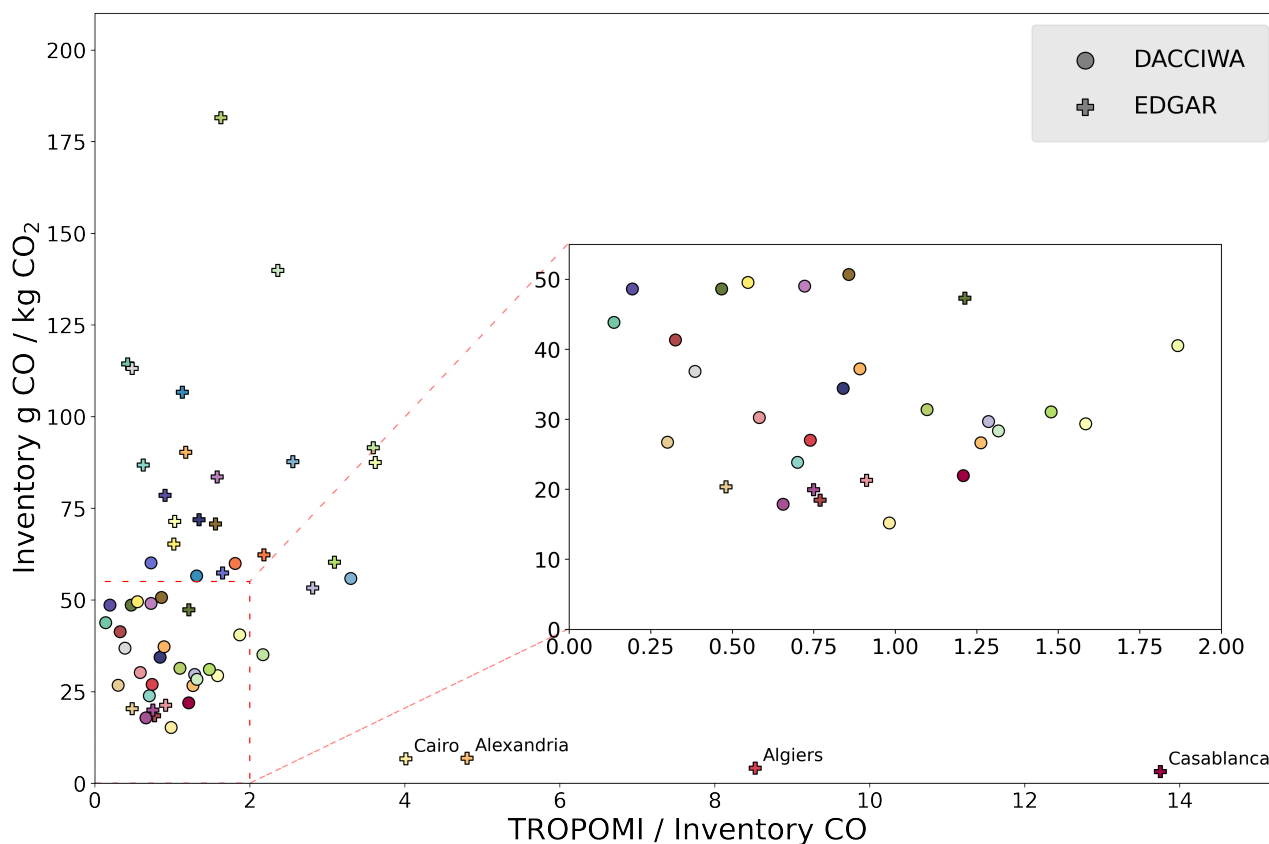


Figure 7. Comparison between inventory combustion completeness and TROPOMI to inventory CO estimates. Each marker represents a single city. As power plants hardly emit any CO per kg of emitted CO₂, the contributions of this sector are removed from the CO₂ values. Cairo, Alexandria, Algiers and Casablanca have very low CO emission rates in EDGAR compared to TROPOMI and compared to EDGAR CO₂ emissions, which indicates that EDGAR largely overestimates the combustion efficiency for these cities. The four cities in EDGAR with CO/CO₂ values around 20 are all cities in South Africa showing lower CO-emission rates than the other African cities.

South Africa

In South Africa we find closer agreement between EDGAR and TROPOMI than in northern Africa. However, the emission rates for the 4 considered cities in DACCIWA are on average 2.4 times higher than those based on TROPOMI (Fig. 6). The emission ratios from Fig. 7 show that the South African cities stand out from the other cities in EDGAR, as they have relatively low CO/CO₂ emission ratios, suggesting high average combustion efficiencies. This does not hold for DACCIWA, where the South African cities have CO/CO₂ emission ratios comparable to other cities. This indicates that the CO emission factors for South Africa are overestimated in DACCIWA, and these cities have higher combustion efficiencies more in line with EDGAR.

235

Nigeria

The four investigated cities in Nigeria show varying results when comparing TROPOMI to the inventories, but the two cities



that stand out are Lagos and Kano. In Lagos we estimate emissions of 0.36 (0.23-0.56) Tg yr⁻¹, that are consistent with EDGAR, but DACCIWA has emissions that are 5.2 times higher. The NCEP winds over Lagos are higher than those in GEOS-FP but less
 240 compatible with the plumes observed by TROPOMI. Even so, the difference between DACCIWA and TROPOMI over Lagos can not be explained by the fact that NCEP winds are higher as the mean difference in wind speed is of the order of 60%. For Kano, in contrast to Lagos, we observe an emission rate of 0.53 (0.41-0.62) Tg yr⁻¹ which is consistent with DACCIWA but more than twice the EDGAR estimate (0.19 Tg yr⁻¹). The CO/CO₂ ratios of the inventories agree within 50% but the differences are caused by the activity data. Figure 8 shows that the CO₂ emission rates in DACCIWA for Lagos, Kano and Ibadan
 245 are respectively 8.1, 3.8 and 3.3 times higher than in EDGAR, this data is also available in appendix in Table D2. Comparing Nigeria's national CO₂ budget there is a 24% difference between the inventories (EDGAR 530 Tg yr⁻¹ to DACCIWA 700 Tg yr⁻¹) but the larger regional discrepancies (over 700% for Lagos' CO₂ emissions) suggest differences in spatial allocation as well.

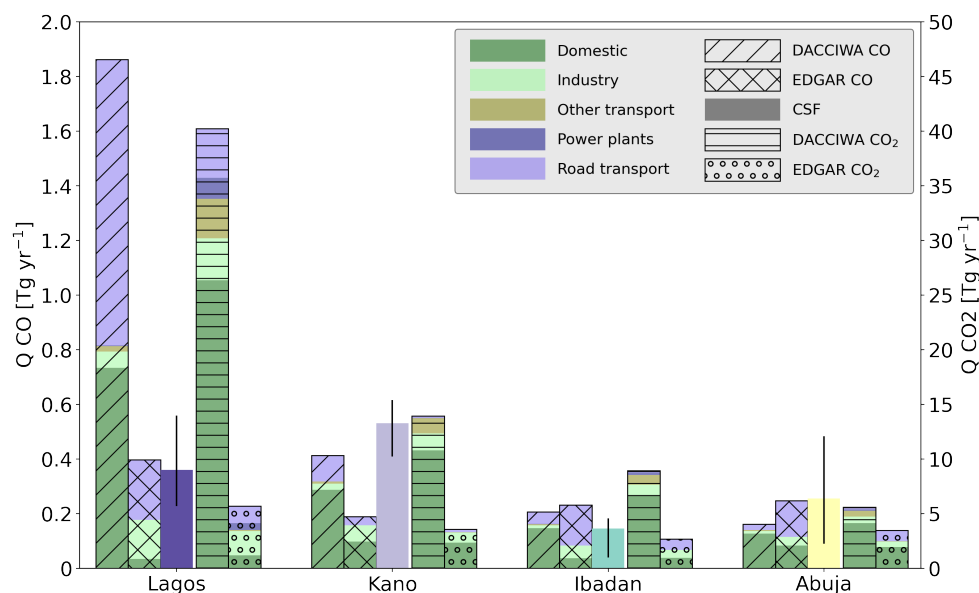


Figure 8. Comparison between the TROPOMI CO emission estimates and EDGAR and DACCIWA CO and CO₂ for four cities in Nigeria with the same color scheme as Fig. 6. The differences between the two inventories in CO₂ emission rates indicate a different spatial allocation - based on gridded activity data- of the national totals.

250 Côte d'Ivoire

Abidjan in Côte d'Ivoire has the largest relative discrepancy between DACCIWA (0.65 Tg yr⁻¹) and TROPOMI (0.1 (0.05-0.16) Tg yr⁻¹). In DACCIWA, the domestic sector contributes for 89% of the city's emissions and Abidjan is the city with one of the highest CO/CO₂ values of all investigated cities. In EDGAR, the domestic CO/CO₂ ratio for Abidjan is four times lower, which would indicate a four times lower emission rate. This would bring the DACCIWA emission rate much closer to



255 the TROPOMI observed emission, indicating that, similar to South Africa, DACCIWA may overestimate the city's domestic
sector's CO emission factor.

Libya

260 Tripoli, the capital of Libya, stands out as its CO emissions in both inventories are almost exclusively (90+%) due to road
transport. The TROPOMI estimate for this city of 0.26 (0.15-0.32) Tg yr⁻¹ is 1.7 and 2.2 times higher than DACCIWA and
EDGAR respectively. The difference can be partly explained by considering the domestic and industry sectors. In both emis-
sion inventories the CO/CO₂ ratios for these sectors are four to five times lower than the mean of the other cities and two
to three times lower than the next lowest city (excluding Egypt, Morocco and Algeria). This implies these sectors in Tripoli
265 to underestimate the emission factor for Tripoli specifically for the non-road transport sectors.

Temporal emission patterns

With the three-year TROPOMI dataset, we can also investigate the temporal variability of emissions. Earlier studies, focusing
on concentration trends rather than emission estimates, have found that CO concentrations over Cairo are lower on Fridays,
270 which is the day off in the Islamic world (Rey-Pommier et al., 2022). This "weekend effect" has also been observed for nitrogen
dioxide (NO₂) and ozone (O₃), which like CO in Cairo are dominated by transport emissions (Beirle et al., 2003; Khoder,
2009; Stavroukou et al., 2020). Combined with the fact that both emission inventories agree on road transport as the main
contributor to emissions in Cairo, lower CO emissions are indeed expected on Fridays when there is less commuter traffic.
Figure 9 indeed shows a 32% drop in emissions on Fridays over Cairo. A similar reduction in emissions can be seen over
275 Algiers, which can also be attributed to reduced road traffic. Similar significant patterns were not seen for the other cities that
tend to have relatively lower contributions from road traffic.

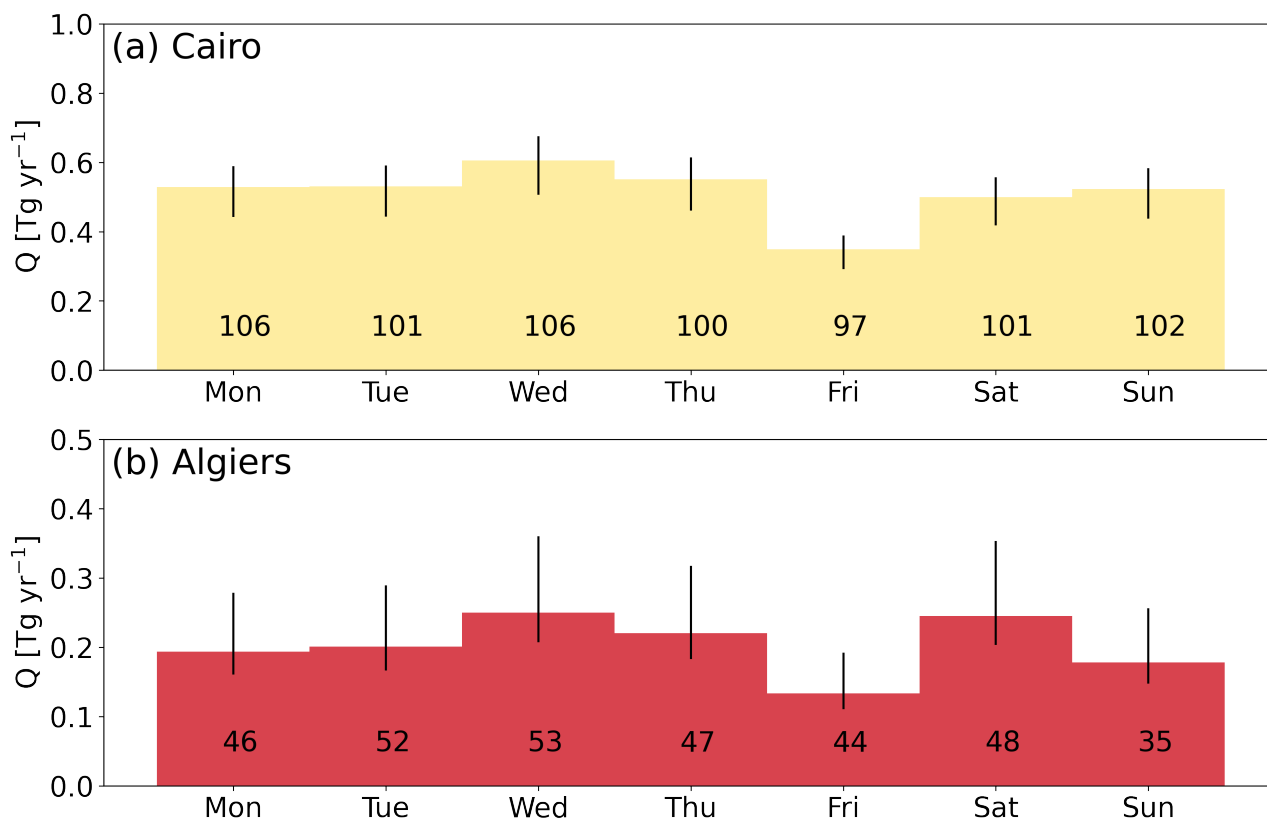


Figure 9. TROPOMI emission estimates over Cairo (panel a) and Algiers (panel b) for different days of the week averaged over 2019-2021. The numbers in the bars show the number of days the averages are based on. Both cities show lower emissions on Friday consistent with road transport being the main contributor to urban emissions and Friday being the standard day off in Islamic countries.

4 Conclusions

We adapted and calibrated the computationally efficient Cross-Sectional Flux (CSF) method to quantify urban carbon monoxide emission rates from major cities in Africa using TROPOMI data. We evaluated the CSF method by applying it to a full-year of WRF simulations over three distinctly different African cities (Cairo, Lagos, and Bamako). These simulations were also used to calibrate the CSF's effective wind speed relationship for TROPOMI data. We found that we can quantify urban CO emissions down to 0.1 Tg yr⁻¹ within 30% uncertainty. After calibration, we applied our CSF method to 29 of Africa's most populated/emitting cities. We focus on Africa as there are relatively few dedicated emission inventories for the continent and large uncertainties in emission rates are expected.

285

We compared our TROPOMI-based emission estimates with the global EDGAR emission inventory and the Africa-focused DACCIIWA inventory. There are substantial differences between urban CO emissions from both inventories. We did not find



290 vastly better average agreement of either inventory with TROPOMI. DACCIWA is closer to the TROPOMI estimate for 16 out of 29 cities. For 10 cities, the DACCIWA and TROPOMI estimates agree within the uncertainty of the TROPOMI-based estimate, but there are also cities with large significant differences of over 600%. Compared to EDGAR, we find 9 cities agree within the uncertainty and we similarly find cities with large discrepancies.

295 We then evaluated our results for different regions. In northern Africa, TROPOMI observes higher emission rates than shown in EDGAR for cities in Egypt, Algeria and Morocco. The EDGAR CO to CO₂ emission ratios for these four cities are relatively low, implying that the mismatch with TROPOMI may originate from the emission factors, which implies that EDGAR would overestimate the average combustion efficiency in these cities. In South-Africa, the TROPOMI estimates agree with EDGAR but the DACCIWA estimates are high in comparison. EDGAR shows lower CO to CO₂ ratios and hence higher combustion efficiency for South Africa compared to other parts of Africa, implying those ratios may be too high in DACCIWA. Similarly, DACCIWA appears to underestimate the combustion efficiency in Abidjan (Côte d'Ivoire). For Tripoli (Libya), both inventories estimate lower emission rates than the estimate based on TROPOMI. Specifically the domestic and industry sectors show particularly high combustion efficiencies compared to other cities in both inventories, which can explain part of the discrepancy.

305 We also found some discrepancies that can be attributed to the activity data used by the inventories. We found a factor ~4 lower emissions based on TROPOMI for Lagos (Nigeria) than estimated by DACCIWA. The associated DACCIWA CO₂ emissions are eight times larger than in EDGAR which can be partly a difference in activity data but also suggests a mismatch related to the spatial distribution of emissions. For Kano (Nigeria) DACCIWA estimates CO₂ emissions that are four times larger than EDGAR. Here, the TROPOMI estimate agrees better with DACCIWA and the activity rate, which corresponds to CO₂ emission, in EDGAR seems to be an underestimation.

310 The large TROPOMI data volume enables identification of temporal emission patterns. Over Cairo and Algiers we find significantly lower emission rates on Fridays - the local rest day - compared to other days of the week. The ability to recognise such patterns builds confidence and shows the strength of TROPOMI's daily global coverage combined with a computationally efficient method like the CSF method developed here.

315 *Code and data availability.* TROPOMI CO data are publicly available at <https://ftp.sron.nl/open-access-data-2/TROPOMI/tropomi/co/>. GEOS-FP wind data can be downloaded at https://gmao.gsfc.nasa.gov/GMAO_products/. ERA5 wind data are available at <https://cds.climate.copernicus.eu>. WRF-Chem code is available at <https://github.com/wrf-model/WRF/releases>, in this work version 4.1.5 was used. EDGAR v5 CO data is available at https://edgar.jrc.ec.europa.eu/dataset_ap50. EDGAR v5 CO₂ data is available at https://edgar.jrc.ec.europa.eu/dataset_ghg50. DACCIWA CO and CO₂ data are available at <https://eccad.aeris-data.fr/> at the Emissions of atmospheric Compounds and Compilation of Ancillary Data (ECCAD) system after creation of a login account. GPW v4 gridded population density is available at <https://sedac.ciesin.columbia.edu/data/set/gpw-v4-population-density-rev11>.

320



Appendix A: TROPOMI-based CO uncertainty

The CSF method as applied in this work has many parameters that were calibrated on simulated plumes. In order to determine the uncertainty of the estimated emission rate we have created an ensemble of emission estimates by varying these parameters. The members of the ensemble and the ranges over which they were varied are shown in Table A1. The wind databases are the three wind products as described in section 2.5 and are responsible for a mean uncertainty of -19% and + 12%. The standard deviation threshold for plume pixels is the number of standard deviations a pixel has to be above the background concentration in order to be considered part of the plume. Pixels identified as part of the plume are only used for fitting the plume shape. The number of cross-sections is the total number of transects drawn perpendicular to the direction of the plume. As described in section 2.4 not all transects are taken into account in the quantification. The number of cross-sections is mostly a measure for the line density, or the distance between consecutive transects as the transects are evenly spaced over the full length of the spline. The minimum pixel coverage is the minimum fraction of a line that needs to be covered by pixels and is a balance between retaining enough days with a valid estimate and not underestimating emissions. A lower limit of 50% coverage per line will retain a lot of lines, and thus, more days with an estimate, however, the cross-sections will potentially miss large parts of the plume. The distance of the background box is important as one would like the box to be close to the city to get a good representation of the local background. However, it must not overlap with any urban emissions to have a clean background. As explained in section 2.4 the location used as center for the emission quantification is shifted upwind to capture the full city plume. The size of this shift is also taken into account in the uncertainty estimate. As a last member of the ensemble we use the spread in emission estimates of the individual transects. We include the means of the transects with the lowest and highest 50% emission rates in the ensemble.

Table A1. Variables used in the uncertainty analysis and the ranges over which they were varied. The resulting ensemble spreads are reported as uncertainty.

Parameter	Domain	Default
Wind database	GEOS-fp 10m, ERA5 10m & GEOS-fp pbl	GEOS-fp 10m
Standard deviation threshold for plume pixels	{1.2 - 2.4}	1.8
Number of transects	{15 - 25}	20
Minimum pixel coverage per transect	{50% - 90%}	70%
Distance of background box	{0.1° - 0.3°}	0.2°
Varying city location upwind	{0° - 0.2°}	0.1°
Transects used for estimate	{Lowest 50% - highest 50%}	All



340 Appendix B: TROPOMI data filtering

Although the CSF has been shown to reproduce simulated emission rates (Fig. 4), it can not be applied to every single overpass of TROPOMI. For example, days with a lot of missing pixels in the TROPOMI data can lead to underestimation of the emission rates. To prevent a positive bias, it is important to not only use days with strong, clearly visible plumes. With the filters chosen in this work, over 400 days are accepted as quantifiable over the 3-year period studied for most non-coastal cities and coastal cities with predominantly inland winds (e.g. Cairo has 713 estimates, Johannesburg 427 and Khartoum 570). With TROPOMI's daily overpasses this means that we estimate emissions on roughly 40% of all days. Regions with fewer estimates tend to be coastal. For example, we only have estimates for 160 days over Lagos and 113 for Dakar because of limited TROPOMI coverage over water. The filters employed are shown in Table B1.

Table B1. Filtering applied to the data to ensure correct application of the CSF method.

Description	Value
Per pixel	
Quality flag TROPOMI (land)	≥ 0.7
Quality flag TROPOMI (water)	$= 0.7$
Per transect	
Misalignment between plume and wind direction	$< 45^\circ$
Minimum pixel coverage	$> 70\%$
Per plume	
Downwind coverage in a $0.3^\circ \times 0.8^\circ$ box	$> 60\%$
Effective wind speed	$> 2\text{m s}^{-1}$
Maximum concentration outside the plume	$< 200\text{ppb}$ (1.5° radius)
Number of transects used for the estimate	> 3
Fraction estimate transect 8-20 to transect 3-7. High emission estimates of the far away lines tend to indicate interference of different sources	$< 2.5\text{x}$
Second derivative of spline scaled to 1° pixel size. This represents the dimensionless curvature of the fitted spline.	< 0.05
Mismatch between the quantification location and the starting pixel of the plume	$< 0.35^\circ$
Fire emission from Global Fire Assimilation System (GFAS) database, (Kaiser et al., 2012)	$< 0.2\text{Tg yr}^{-1}$ (0.75° radius) $< 0.5\text{Tg yr}^{-1}$ (1.5° radius)



Appendix C: CSF estimates

Table C1. Emission estimates for the studied African cities by applying the CSF method to the TROPOMI CO product (2019-2021) as well as the corresponding emission rates according to the DACCIWA (2015) and EDGAR (2015) inventories. All emission rates are in Tg yr^{-1} . Population is taken from the Center for International Earth Science Information Network CIESIN (2018)

City	Country	Population	TROPOMI estimate	Lower limit	Upper limit	DACCIWA	EDGAR
Algiers	Algeria	4.2M	0.213	0.177	0.307	0.288	0.025
Luanda	Angola	5.1M	0.268	0.166	0.413	0.489	0.263
Ouagadougou	Burkina Faso	2.8M	0.273	0.243	0.335	0.126	0.076
Kinshasa	Congo	7.4M	0.628	0.49	0.894	0.477	0.266
Abidjan	Côte d'Ivoire	7.1M	0.09	0.054	0.157	0.654	0.266
Alexandria	Egypt	3.3M	0.197	0.164	0.257	0.156	0.041
Cairo	Egypt	16.7M	0.546	0.456	0.608	0.556	0.136
Addis Ababa	Ethiopia	4.4M	0.239	0.2	0.295	0.268	0.204
Accra	Ghana	3.5M	0.194	0.176	0.318	0.148	0.172
Nairobi	Kenya	4.8M	0.17	0.153	0.247	0.441	0.353
Tripoli	Libya	1.2M	0.264	0.151	0.32	0.146	0.121
Antananarivo	Madagascar	3.0M	0.135	0.104	0.156	0.123	0.083
Casablanca	Morocco	4.2M	0.11	0.078	0.171	0.091	0.008
Maputo	Mozambique	2.5M	0.151	0.125	0.199	0.176	0.097
Abuja	Nigeria	2.6M	0.255	0.089	0.483	0.161	0.247
Ibadan	Nigeria	2.2M	0.145	0.039	0.183	0.207	0.232
Kano	Nigeria	5.3M	0.531	0.409	0.616	0.413	0.189
Lagos	Nigeria	10.9M	0.36	0.227	0.558	1.862	0.397
Dakar	Senegal	4.2M	0.293	0.154	0.381	0.157	0.081
Cape Town	South Africa	4.1M	0.189	0.155	0.252	0.288	0.252
Durban	South Africa	3.3M	0.157	0.132	0.233	0.482	0.204
Johannesburg	South Africa	9.1M	0.232	0.184	0.291	0.77	0.482
Pretoria	South Africa	6.4M	0.197	0.139	0.209	0.338	0.216
Khartoum	Sudan	3.1M	0.396	0.336	0.432	0.12	0.155
Dar es Salaam	Tanzania	5.4M	0.286	0.241	0.496	0.396	0.181
Kampala	Uganda	4.3M	0.362	0.279	0.431	0.245	0.117
Lusaka	Zambia	2.4M	0.226	0.108	0.23	0.269	0.168
Bulawayo	Zimbabwe	0.8M	0.094	0.043	0.111	0.13	0.057
Harare	Zimbabwe	2.7M	0.142	0.076	0.157	0.304	0.117



350 Appendix D: Inventory emission rates

Table D1. Sectoral breakdown of the CO emission rates for the studied African cities according to the DACCIWA and EDGAR inventory. All emission rates are in Gg yr⁻¹.

City	DACCIWA					EDGAR				
	Domestic	Industry	Other	Power	Road	Domestic	Industry	Other	Power	Road
Algiers	0.3	33.7	0.6	0.9	252.2	1.3	2.7	0.2	0.4	20.0
Luanda	326.1	19.4	12.0	3.4	129.0	25.4	174.0	0.3	6.5	56.1
Ouagadougou	90.3	8.0	0.0	0.8	26.4	13.2	39.8	0.1	2.8	20.0
Kinshasa	411.1	25.4	0.0	0.0	40.4	20.1	222.3	0.1	0.1	23.5
Abidjan	579.9	21.4	20.4	7.0	25.5	10.8	183.6	0.3	1.6	15.7
Alexandria	24.3	46.7	20.7	4.4	59.6	3.4	1.8	0.3	15.8	19.9
Cairo	75.8	145.5	64.6	26.1	244.3	3.5	6.4	1.1	9.3	115.9
Addis Ababa	245.3	8.5	1.8	0.0	12.3	55.3	134.8	0.2	0.0	13.9
Accra	108.2	3.2	3.9	0.0	32.4	5.0	90.2	1.0	0.5	43.2
Nairobi	370.8	11.7	0.2	2.3	59.1	23.5	266.9	0.3	2.1	60.0
Tripoli	3.1	4.2	0.0	6.6	131.6	1.9	0.1	0.1	0.0	118.9
Antananarivo	68.8	17.0	30.2	0.1	6.5	7.5	68.3	0.1	0.0	7.3
Casablanca	29.2	37.1	4.6	0.5	20.0	1.5	3.9	0.0	0.2	2.2
Maputo	153.1	5.3	0.1	3.1	14.7	21.0	62.7	0.0	0.3	13.1
Abuja	126.2	10.2	3.6	0.1	21.0	82.6	32.1	0.0	0.0	131.9
Ibadan	145.8	11.7	4.1	0.3	44.7	36.2	46.4	0.0	0.0	149.1
Kano	286.3	23.0	8.1	0.0	95.5	96.9	60.6	0.0	0.0	31.0
Lagos	733.5	59.0	20.8	2.4	1046.3	33.2	143.5	0.1	0.7	219.8
Dakar	123.3	17.4	0.1	6.1	10.0	2.7	62.7	0.2	3.2	12.6
Cape Town	139.9	50.7	5.7	1.4	90.5	56.9	170.1	0.7	0.0	23.8
Durban	183.8	66.6	7.5	0.0	224.4	53.3	139.4	0.3	0.0	10.9
Johannesburg	355.8	128.9	14.5	22.4	247.9	108.8	317.5	0.1	0.0	55.1
Pretoria	180.4	65.4	7.4	0.9	83.4	57.3	129.0	0.1	0.4	29.3
Khartoum	77.2	10.8	3.8	1.6	26.2	16.3	90.0	0.1	5.6	42.6
Dar es Salaam	354.2	15.0	9.6	1.7	15.8	15.1	138.1	0.1	10.4	17.7
Kampala	198.8	10.5	0.1	1.2	34.2	65.6	42.5	0.0	0.0	8.8
Lusaka	239.0	11.7	1.2	0.0	16.7	31.7	126.3	0.0	0.0	9.8
Bulawayo	79.1	4.3	3.5	0.2	42.4	21.5	2.0	0.0	0.2	33.0
Harare	248.2	13.3	10.8	0.2	31.5	69.8	4.5	0.1	0.4	41.7



Table D2. Sectoral breakdown of the CO₂ emission rates for the studied African cities according to the DACCIWA and EDGAR inventory.

All emission rates are in Tg yr⁻¹.

City	DACCIWA					EDGAR				
	Domestic	Industry	Other	Power	Road	Domestic	Industry	Other	Power	Road
Algiers	2.0526	2.3547	0.3026	0.7006	5.9577	2.2141	2.3123	0.1231	0.0446	1.4081
Luanda	4.8853	1.4104	2.2871	0.0	1.2816	1.8331	1.4681	0.1276	1.6398	0.6036
Ouagadougou	2.1571	0.5752	0.701	0.4603	0.1553	0.3469	0.2106	0.1102	0.4868	0.1633
Kinshasa	9.1058	2.4811	4.9228	0.0	0.3205	0.4757	1.1183	0.0897	0.0245	0.2184
Abidjan	5.6168	1.2141	7.6905	4.1632	0.3916	0.3994	1.1479	0.1115	1.1956	0.1948
Alexandria	1.7076	3.1371	0.3293	0.0	0.6755	0.8145	4.1211	0.0639	23.3842	0.9927
Cairo	9.7364	17.8872	3.5146	17.7906	5.4195	3.1328	11.4975	0.7648	13.7938	4.9941
Addis Ababa	5.2452	0.4889	1.0817	0.0	0.3851	1.2733	0.5438	0.2141	0.0005	0.2297
Accra	1.172	0.3122	0.7803	0.6024	0.3533	0.231	0.6034	0.4059	0.3562	0.3729
Nairobi	5.3718	0.9503	4.7633	0.429	0.8817	0.6676	1.6001	0.2878	0.4414	0.5657
Tripoli	0.3477	0.8711	0.3068	7.4683	0.9077	0.252	0.6718	0.022	0.0	0.9969
Antananarivo	1.7812	0.9208	1.0695	0.0798	0.1474	0.205	0.144	0.046	0.0195	0.0622
Casablanca	1.4466	2.1949	0.0158	4.0377	0.4885	0.7635	1.2911	0.0514	1.2078	0.3914
Maputo	2.3379	0.2568	0.6895	0.0	0.1877	0.4888	0.7266	0.0355	0.0795	0.1202
Abuja	4.1275	0.6013	0.5368	0.1024	0.2142	1.9347	0.4962	0.0413	0.0	0.9858
Ibadan	6.678	0.9728	0.8684	0.2404	0.1572	0.944	0.7214	0.0006	0.0006	1.0063
Kano	10.773	1.5693	1.401	0.0311	0.1601	2.3444	0.9346	0.0206	0.0008	0.2502
Lagos	26.3529	3.8388	3.5988	1.9078	4.5136	1.1902	2.2007	0.0889	0.6383	1.5765
Dakar	1.5405	1.01	0.9282	1.9502	0.3954	0.1379	0.4475	0.1115	1.2811	0.2292
Cape Town	3.1332	10.8663	1.2788	1.0896	0.823	1.759	9.0686	0.247	0.0009	1.5695
Durban	2.3207	8.0484	0.543	0.1116	0.7436	1.5599	8.5055	0.0943	0.1335	0.9045
Johannesburg	5.5358	19.1984	2.2775	23.3095	1.7699	3.1791	17.0838	0.1623	4.9948	3.2495
Pretoria	2.2686	7.8676	0.5308	3.0576	0.5046	1.6006	6.6839	0.1254	3.4728	1.7434
Khartoum	0.6315	0.9569	0.3614	0.1673	0.198	0.5049	0.6555	0.101	1.4848	0.5062
Dar es Salaam	5.582	1.0448	1.4222	1.073	0.0259	0.3639	1.5205	0.0908	1.3461	0.1923
Kampala	5.0997	0.8774	1.6523	0.5054	0.2586	1.4997	0.329	0.009	0.0	0.1042
Lusaka	3.8478	1.6338	2.2394	0.0	0.0951	0.7361	1.4979	0.0327	0.0	0.0699
Bulawayo	1.8723	0.1759	0.0062	0.2274	0.1068	0.5132	0.2041	0.0134	0.2151	0.263
Harare	5.522	0.5187	0.0183	0.2416	0.193	1.6508	0.3461	0.059	0.4645	0.4179



Author contributions. GL, JDM, and IA designed the study. GL performed the TROPOMI analysis with contributions from JDM, HDG AS and IA. GL and JDM wrote the paper with contributions from all authors. JDM, HDG and AS contributed to the comparison between TROPOMI and emission inventories. TB provided the TROPOMI carbon monoxide data and associated support.

Competing interests. The authors declare that they have no competing interests.

355 *Acknowledgements.* We thank the team that realized the TROPOMI instrument and its data products, consisting of the partnership between Airbus Defence and Space Netherlands, KNMI, SRON, and TNO, commissioned by NSO and ESA. Sentinel-5 Precursor is part of the EU Copernicus program, and Copernicus Sentinel-5P data (2019-2021) have been used. We thank SURF (www.surf.nl) for the support in using the National Supercomputer Snellius. This research was partly funded by the European Commission, Horizon 2020 Framework Programme (CoCO2 project (grant no. 958927)). We thank Sekou Keita and Cathy Liousse (CNRS, Toulouse) for development and early access to the
360 DACCWA_v2 dataset.



References

- Badarinath, K., Kharol, S. K., Chand, T. K., Parvathi, Y. G., Anasuya, T., and Jyothsna, A. N.: Variations in black carbon aerosol, carbon monoxide and ozone over an urban area of Hyderabad, India, during the forest fire season, *Atmospheric Research*, 85, 18–26, 2007.
- Beirle, S., Platt, U., Wenig, M., and Wagner, T.: Weekly cycle of NO₂ by GOME measurements: a signature of anthropogenic sources, *Atmospheric Chemistry and Physics*, 3, 2225–2232, 2003.
- 365 Bi, J., Zuidema, C., Clausen, D., Kirwa, K., Young, M. T., Gassett, A. J., Seto, E. Y., Sampson, P. D., Larson, T. V., Szpiro, A. A., et al.: Within-City Variation in Ambient Carbon Monoxide Concentrations: Leveraging Low-Cost Monitors in a Spatiotemporal Modeling Framework, *Environmental Health Perspectives*, 130, 097 008, 2022.
- Borsdorff, T., Aan de Brugh, J., Hu, H., Aben, I., Hasekamp, O., and Landgraf, J.: Measuring carbon monoxide with TROPOMI: First results and a comparison with ECMWF-IFS analysis data, *Geophysical Research Letters*, 45, 2826–2832, 2018.
- 370 Borsdorff, T., García Reynoso, A., Maldonado, G., Mar-Morales, B., Stremme, W., Grutter, M., and Landgraf, J.: Monitoring CO emissions of the metropolis Mexico City using TROPOMI CO observations, *Atmospheric Chemistry and Physics*, 20, 15 761–15 774, 2020.
- Cai, B., Cui, C., Zhang, D., Cao, L., Wu, P., Pang, L., Zhang, J., and Dai, C.: China city-level greenhouse gas emissions inventory in 2015 and uncertainty analysis, *Applied energy*, 253, 113 579, 2019.
- 375 CIESIN: Gridded Population of the World, Version 4 (GPWv4): Population Density, Revision 11., <https://doi.org/10.7927/H49C6VHW>, accessed: 2021-04-01, 2018.
- Daniel, J. S. and Solomon, S.: On the climate forcing of carbon monoxide, *Journal of Geophysical Research: Atmospheres*, 103, 13 249–13 260, 1998.
- Dekker, I., Houweling, S., Aben, I., Roeckmann, T., and Krol, M.: Quantification of point sources of carbon monoxide using satellite measurements, in: EGU General Assembly Conference Abstracts, p. 13167, 2017.
- 380 Eggleston, H., Buendia, L., Miwa, K., Ngara, T., and Tanabe, K.: 2006 IPCC guidelines for national greenhouse gas inventories, 2006.
- Guevara, M., Jorba, O., Tena, C., Denier van der Gon, H., Kuenen, J., Elguindi, N., Darras, S., Granier, C., and Pérez García-Pando, C.: Copernicus Atmosphere Monitoring Service TEMPORal profiles (CAMS-TEMPO): global and European emission temporal profile maps for atmospheric chemistry modelling, *Earth System Science Data*, 13, 367–404, 2021.
- 385 Hannigan, J.: Ndacc irwg: Evolution of ground-based global trace gas infrared remote sensing, in: *Fourier Transform Spectroscopy*, p. FMC1, Optica Publishing Group, 2011.
- Hedelius, J. K., Toon, G. C., Buchholz, R. R., Iraci, L. T., Podolske, J. R., Roehl, C. M., Wennberg, P. O., Worden, H. M., and Wunch, D.: Regional and urban column CO trends and anomalies as observed by MOPITT over 16 years, *Journal of Geophysical Research: Atmospheres*, 126, e2020JD033 967, 2021.
- 390 Hersbach, H., Bell, B., Berrisford, P., Hirahara, S., Horányi, A., Muñoz-Sabater, J., Nicolas, J., Peubey, C., Radu, R., Schepers, D., et al.: The ERA5 global reanalysis, *Quarterly Journal of the Royal Meteorological Society*, 146, 1999–2049, 2020.
- Hoornweg, D. and Pope, K.: Population predictions for the world's largest cities in the 21st century, *Environment and Urbanization*, 29, 195–216, 2017.
- Inness, A., Blechschmidt, A.-M., Bouarar, I., Chabrilat, S., Crepulja, M., Engelen, R., Eskes, H., Flemming, J., Gaudel, A., Hendrick, F., et al.: Data assimilation of satellite-retrieved ozone, carbon monoxide and nitrogen dioxide with ECMWF's Composition-IFS, *Atmospheric chemistry and physics*, 15, 5275–5303, 2015.
- 395



- IPCC: Climate Change and Land: an IPCC special report on climate change, desertification, land degradation, sustainable land management, food security, and greenhouse gas fluxes in terrestrial ecosystems, In press., 2019.
- Jacob, D. J.: Introduction to atmospheric chemistry, Princeton University Press, 1999.
- 400 Janssens-Maenhout, G., Crippa, M., Guizzardi, D., Muntean, M., Schaaf, E., Dentener, F., Bergamaschi, P., Pagliari, V., Olivier, J. G., Peters, J. A., et al.: EDGAR v4. 3.2 Global Atlas of the three major greenhouse gas emissions for the period 1970–2012, *Earth System Science Data*, 11, 959–1002, 2019.
- Kaiser, J., Heil, A., Andreae, M., Benedetti, A., Chubarova, N., Jones, L., Morcrette, J.-J., Razinger, M., Schultz, M., Suttie, M., et al.: Biomass burning emissions estimated with a global fire assimilation system based on observed fire radiative power, *Biogeosciences*, 9, 405 527–554, 2012.
- Keita, S., Lioussé, C., Assamoi, E.-M., Doumbia, T., N'Datchoh, E. T., Gnamien, S., Elguindi, N., Granier, C., and Yoboué, V.: African anthropogenic emissions inventory for gases and particles from 1990 to 2015, *Earth System Science Data*, 13, 3691–3705, 2021.
- Khoder, M. I.: Diurnal, seasonal and weekdays–weekends variations of ground level ozone concentrations in an urban area in greater Cairo, *Environmental Monitoring and Assessment*, 149, 349–362, 2009.
- 410 Lama, S., Houweling, S., Boersma, K. F., Aben, I., van der Gon, H., Krol, M. C., Dolman, H., Borsdorff, T., and Lorente, A.: Quantifying burning efficiency in megacities using NO₂/CO ratio from the tropospheric monitoring instrument (TROPOMI), *Atmos. Chem. Phys. Discuss*, 1, 2019.
- Landgraf, J., de Brugh, J., Scheepmaker, R., Borsdorff, T., Houweling, S., and Hasekamp, O.: Algorithm theoretical baseline document for sentinel-5 precursor: Carbon monoxide total column retrieval, Netherlands: Netherlands Institute for Space Research, 2018.
- 415 Macknick, J.: Energy and CO₂ emission data uncertainties, *Carbon Management*, 2, 189–205, 2011.
- McKain, K., Wofsy, S. C., Nehrkorn, T., Eluszkiewicz, J., Ehleringer, J. R., and Stephens, B. B.: Assessment of ground-based atmospheric observations for verification of greenhouse gas emissions from an urban region, *Proceedings of the National Academy of Sciences*, 109, 8423–8428, 2012.
- Molod, A., Takacs, L., Suarez, M., Bacmeister, J., Song, I.-S., and Eichmann, A.: The GEOS-5 atmospheric general circulation model: Mean 420 climate and development from MERRA to Fortuna, Tech. rep., 2012.
- NCEP: NCEP FNL Operational Model Global Tropospheric Analyses, <https://doi.org/10.5065/D6M043C6>, 2000.
- Nielsen, O.-K.: EMEP/EEA air pollutant emission inventory guidebook 2013. Technical guidance to prepare national emission inventories, 2013.
- Oda, T., Bun, R., Kinakh, V., Topylko, P., Halushchak, M., Marland, G., Lauvaux, T., Jonas, M., Maksyutov, S., Nahorski, Z., et al.: Errors and 425 uncertainties in a gridded carbon dioxide emissions inventory, *Mitigation and Adaptation Strategies for Global Change*, 24, 1007–1050, 2019.
- Oreggioni, G. D., Ferrario, F. M., Crippa, M., Muntean, M., Schaaf, E., Guizzardi, D., Solazzo, E., Duerr, M., Perry, M., and Vignati, E.: Climate change in a changing world: Socio-economic and technological transitions, regulatory frameworks and trends on global greenhouse gas emissions from EDGAR v. 5.0, *Global Environmental Change*, 70, 102 350, 2021.
- 430 Pandey, S., Gautam, R., Houweling, S., Van Der Gon, H. D., Sadavarte, P., Borsdorff, T., Hasekamp, O., Landgraf, J., Tol, P., Van Kempen, T., et al.: Satellite observations reveal extreme methane leakage from a natural gas well blowout, *Proceedings of the National Academy of Sciences*, 116, 26 376–26 381, 2019.
- Park, H., Jeong, S., Park, H., Labzovskii, L. D., and Bowman, K. W.: An assessment of emission characteristics of Northern Hemisphere cities using spaceborne observations of CO₂, CO, and NO₂, *Remote Sensing of Environment*, 254, 112 246, 2021.



- 435 Plant, G., Kort, E. A., Murray, L. T., Maasackers, J. D., and Aben, I.: Evaluating urban methane emissions from space using TROPOMI methane and carbon monoxide observations, *Remote Sensing of Environment*, 268, 112 756, 2022.
- Powers, J. G., Klemp, J. B., Skamarock, W. C., Davis, C. A., Dudhia, J., Gill, D. O., Coen, J. L., Gochis, D. J., Ahmadov, R., Peckham, S. E., et al.: The weather research and forecasting model: Overview, system efforts, and future directions, *Bulletin of the American Meteorological Society*, 98, 1717–1737, 2017.
- 440 Qu, Z., Henze, D. K., Worden, H. M., Jiang, Z., Gaubert, B., Theys, N., and Wang, W.: Sector-based top-down estimates of NO_x, SO₂, and CO emissions in East Asia, *Geophysical Research Letters*, 49, e2021GL096 009, 2022.
- Rey-Pommier, A., Chevallier, F., Ciais, P., Broquet, G., Christoudias, T., Kushta, J., Hauglustaine, D., and Sciare, J.: Quantifying NO_x emissions in Egypt using TROPOMI observations, *Atmospheric Chemistry and Physics Discussions*, pp. 1–21, 2022.
- 445 Sadavarte, P., Pandey, S., Maasackers, J. D., Lorente, A., Borsdorff, T., Denier van der Gon, H., Houweling, S., and Aben, I.: Methane emissions from superemitting coal mines in Australia quantified using TROPOMI satellite observations, *Environmental Science & Technology*, 55, 16 573–16 580, 2021a.
- Sadavarte, P., Pandey, S., Maasackers, J. D., Lorente, A., Borsdorff, T., Denier van der Gon, H., Houweling, S., and Aben, I.: Methane emissions from superemitting coal mines in Australia quantified using TROPOMI satellite observations, *Environmental Science & Technology*, 55, 16 573–16 580, 2021b.
- 450 Sha, M. K., Langerock, B., Blavier, J.-F. L., Blumenstock, T., Borsdorff, T., Buschmann, M., Dehn, A., De Mazière, M., Deutscher, N. M., Feist, D. G., et al.: Validation of methane and carbon monoxide from Sentinel-5 Precursor using TCCON and NDACC-IRWG stations, *Atmospheric Measurement Techniques*, 14, 6249–6304, 2021.
- Silva, S. J., Arellano, A. F., and Worden, H. M.: Toward anthropogenic combustion emission constraints from space-based analysis of urban CO₂/CO sensitivity, *Geophysical Research Letters*, 40, 4971–4976, 2013.
- 455 Stavrakou, T., Müller, J.-F., Bauwens, M., Boersma, K., and Van Geffen, J.: Satellite evidence for changes in the NO₂ weekly cycle over large cities, *Scientific reports*, 10, 1–9, 2020.
- Tian, Y., Liu, C., Sun, Y., Borsdorff, T., Landgraf, J., Lu, X., Palm, M., and Notholt, J.: Satellite observations reveal a large CO emission discrepancy from industrial point sources over China, *Geophysical Research Letters*, 49, e2021GL097 312, 2022a.
- Tian, Y., Sun, Y., Borsdorff, T., Liu, C., Liu, T., Zhu, Y., Yin, H., and Landgraf, J.: Quantifying CO emission rates of industrial point sources from Tropospheric Monitoring Instrument observations, *Environmental Research Letters*, 17, 014 057, 2022b.
- 460 Varon, D. J., Jacob, D. J., McKeever, J., Jervis, D., Durak, B. O., Xia, Y., and Huang, Y.: Quantifying methane point sources from fine-scale satellite observations of atmospheric methane plumes, *Atmospheric Measurement Techniques*, 11, 5673–5686, 2018.
- Varon, D. J., Jacob, D. J., Jervis, D., and McKeever, J.: Quantifying time-averaged methane emissions from individual coal mine vents with GHGSat-D satellite observations, *Environmental Science & Technology*, 54, 10 246–10 253, 2020.
- 465 Veefkind, J., Aben, I., McMullan, K., Förster, H., De Vries, J., Otter, G., Claas, J., Eskes, H., De Haan, J., Kleipool, Q., et al.: TROPOMI on the ESA Sentinel-5 Precursor: A GMES mission for global observations of the atmospheric composition for climate, air quality and ozone layer applications, *Remote sensing of environment*, 120, 70–83, 2012.
- Wu, D., Liu, J., Wennberg, P. O., Palmer, P. I., Nelson, R. R., Kiel, M., and Eldering, A.: Towards sector-based attribution using intra-city variations in satellite-based emission ratios between CO₂ and CO, *Atmospheric Chemistry and Physics Discussions*, pp. 1–32, 2022.
- 470 Wuebbles, D. J. and Hayhoe, K.: Atmospheric methane and global change, *Earth-Science Reviews*, 57, 177–210, 2002.



- Wunch, D., Toon, G. C., Blavier, J.-F. L., Washenfelder, R. A., Notholt, J., Connor, B. J., Griffith, D. W., Sherlock, V., and Wennberg, P. O.:
The total carbon column observing network, *Philosophical Transactions of the Royal Society A: Mathematical, Physical and Engineering
Sciences*, 369, 2087–2112, 2011.
- Yumimoto, K., Uno, I., and Itahashi, S.: Long-term inverse modeling of Chinese CO emission from satellite observations, *Environmental
475 pollution*, 195, 308–318, 2014.
- Zhong, Q., Huang, Y., Shen, H., Chen, Y., Chen, H., Huang, T., Zeng, E. Y., and Tao, S.: Global estimates of carbon monoxide emissions
from 1960 to 2013, *Environmental Science and Pollution Research*, 24, 864–873, 2017.